Journal of
Mechanical
Science and
Technology

Journal of Mechanical Science and Technology 21 (2007) 1847~1854

Numerical analysis of crater formation and ablation depth in thin silicon films heated by ultrashort pulse train lasers

Hyung Sub Sim[1], Seong Hyuk Lee[1,*] and Joon Sik Lee[2]

[1]*School of Mechanical Engineering, Chung-Ang University, Seoul, Korea*
[2]*School of Mechanical and Aerospace Engineering, Seoul National University, Seoul, Korea*

(Manuscript Received May 7, 2007; Revised August 6, 2007; Accepted July 6, 2007)

Abstract

This study numerically investigates the optical and heat transfer characteristics of thin silicon films irradiated by ultrashort (shorter than 10 ps) pulse train lasers. The one-dimensional two-temperature model (1DTTM) is extended to the two-dimensional (2DTTM) model for estimation of crater formation. In addition, the wave interference effects on the optical and energy transfer characteristics are considered to predict accurately the energy absorption rates in thin silicon films irradiated by picosecond-to-femtosecond pulse train lasers. Unlike bulk silicon, a significant change in energy absorption is found to occur in thin silicon films with the variation of film thickness due to the wave interference. The spatial distributions of energy carrier and lattice temperature show quite a different tendency at different pulse durations as well as the number of pulses because of significant changes in the optical and thermal properties. The predicted crater shapes and the ablation depths by 2DTTM are also presented.

Keywords: Ultrashort pulse train lasers; Wave interference; Ablation; Crater; Heat transfer

1. Introduction

Ultrashort pulse train lasers have received considerable attention due to their convenience in micro-analytics, material processing with high precision, and microelectronic technology [1]. In particular, the ultrashort pulse train lasers are powerful tools for extremely precise micro-nano fabrication of almost any kind of material because they have features of the laser-solid interactions, such as minimizing laser-plume interaction and reducing the heat-affected zone [2-7]. For the applications listed above, understanding of heat transfer characteristics and energy transport mechanism from laser-induced material is of crucial importance. Extensive efforts have been devoted to theoretical and experimental researches of laser-solid interactions in recent years [2-20]. Nevertheless, the mechanisms of laser ablation for different materials such as metals, semiconductors, and dielectrics have been still debated and poorly understood in the pico- to- femtosecond pulse train laser process.

Many researchers have discussed the ultrashort pulse laser-induced excitation of energy carriers in both electron and lattice systems on the assumption of the local quasi-equilibrium [4-12, 16-20]. The carrier number density, electron temperature, and lattice temperature are estimated on the relaxation time approximation to the Boltzmann transport equation. When the pulse duration is comparable to 100 fs, the two-temperature model can be valid because the electron-lattice energy relaxation time is about 0.5 ps. Furthermore, during pulse train laser irradiation, the optical properties of thin films are changed with temperature and carrier number density [5-6, 12-14, 17], causing a change in the reflectivity and the absorption coefficients. In particular, for thin silicon film structures, the wave interference effect can be dominant as the film thickness decreases. This plays an important role in determining the absorbed energy

*Corresponding author. Tel.: +82 2 820 5254, Fax.: +82 2 823 9780
E-mail address: shlee89@cau.ac.kr

propagation in silicon films [21-23]. Choi et al. [17] investigated the mechanism of femtosecond pulse laser-induced ablation on the silicon wafers, and they compared the melting depth predicted by the two temperature model (TTM) with the experimental observation of the crater shape. Burakov et al. [2] proposed a new TTM on the basis of the drift-diffusion approach to describe the dynamics of electronic excitation and lattice heating in dielectrics. They showed the predicted crater shapes which were generated in fused silica and sapphire during irradiation from a femtosecond pulse train laser.

The ultimate goal of this study is to investigate the energy transport and the optical characteristics of thin silicon films irradiated by pico-to-femtosecond pulse train lasers. The variations of carrier number density, electron temperature, and lattice temperature are explained from the viewpoint of some important factors such as pulse duration time, number of pulse, and laser fluence. In fact, the previous 1DTTM cannot intrinsically predict the ablated crater formation of silicon films [7-12, 16-21]. Thus, this study extends the previous 1DTTM to the two-dimensional model (2DTTM) for the direct comparison with experimental data of the crater shape and depth. Moreover, the characteristic transmission matrix (CTM) method from thin film optics in stratified media is utilized to estimate laser energy absorption according to the variation of the complex refractive index due to the wave interference.

2. Mathematical representation and computational details

Under ultrashort pulse laser irradiation, the present study uses the balance equation of the carrier number density N to describe the change of the carrier number density due to photon energy absorption as follows [19, 20];

$$\frac{\partial N}{\partial t}=\frac{\partial}{\partial x}\left(D_0\frac{\partial N}{\partial x}\right)+\frac{\partial}{\partial y}\left(D_0\frac{\partial N}{\partial y}\right) -\gamma N^3+\delta(T_e)N+G(x,y,t) \tag{1}$$

$$G(x,y,t)=\frac{\alpha I}{\hbar\omega}+\frac{\beta I^2}{2\hbar\omega} \tag{2}$$

where D_0 is the ambipolar diffusivity, γ is Auger recombination coefficient, and $\delta(T_e)$ indicates the dependence of the impact ionization coefficient on the electron temperature. G represents the laser absorption source term. In Eq. (2), α is linear absorption coefficient, β is the two-photon absorption coefficient, and $\hbar\omega$ is the photon energy quantum. For a wavelength of 530 nm, the two-photon absorption coefficient can be neglected [20]. In the present study, the linear absorption should only be considered. The pulse train laser consists of a sequence of the laser pulses with the laser intensity profiles $I(x, y, t)$ of the Gaussian temporal and spatial form as follows [24];

$$I(x,y,t)=\frac{0.94J(1-R)}{t_p}\exp\left(-\int_0^z(\alpha+\theta N)dz\right) \times\exp\left(-\frac{r^2}{r_0^2}-2.773\frac{t^2}{t_p^2}\right) \tag{3}$$

where J is the laser fluence, R reflectivity, θ free carrier absorption coefficient, r_0 the laser beam spot size, and t_p denotes the pulse duration time.

The present study employs the relaxation time approximation to Boltzmann's transport equation and assumes a single thermodynamics system where optical phonons and acoustic phonons are in the equilibrium state. The electron and lattice energy conservation equations can be described as follows [19, 20]:

$$\frac{\partial U_e}{\partial t}=\frac{\partial}{\partial x}\left(k_e\frac{\partial T_e}{\partial x}\right)+\frac{\partial}{\partial y}\left(k_e\frac{\partial T_e}{\partial y}\right) -\frac{3Nk_B}{\tau_{e-l}}(T_e-T_l)+\dot{q}_{tot} \tag{4}$$

$$\frac{\partial U_l}{\partial t}=\frac{\partial}{\partial x}\left(k_l\frac{\partial T_l}{\partial x}\right)+\frac{\partial}{\partial y}\left(k_l\frac{\partial T_l}{\partial y}\right) +\frac{3Nk_B}{\tau_{e-l}}(T_e-T_l) \tag{5}$$

where U_e and U_l are the electron and lattice internal energies, respectively. τ_{e-l} is the electron-lattice relaxation time, and $\dot{q}_{tot}$ is the total laser absorption source term.

The reflectivity and the absorption coefficient are continuously changed during the laser irradiation because of the variation of the electron density and lattice temperature [5-6, 12-14, 17]. Conse-quently, this change directly affects the absorption charac-

teristics of laser energy inside the material. The laser energy absorption in silicon films is estimated by the thin film optics from which the characteristics transmission matrix (CTM) method is derived in stratified media, considering a rapid change in complex refractive index due to wave interference effects [21-23]. The energy source term in Eq. (4) can be determined from

$$\dot{q}_{tot} = I(x,0,t)\frac{dS_m}{dy} \tag{6}$$

where S_m indicates the local energy flow of Poynting vectors which is normalized by incident energy flux on the thin film structure. The laser absorption includes linear absorption and free carrier absorption. For solving the balance equation of the carrier number density, however, only linear absorption should be considered. Thus, in order to separate the linear absorption part from the total absorption term, the present study uses a relationship of linear absorption involving the imaginary part of dielectric function from the literature [25].

$$\dot{q}_{\text{linear absorption}} = \frac{\text{Im}(\dot{\varepsilon}_{Si})}{\text{Im}(\dot{\varepsilon})}\dot{q}_{tot} \tag{7}$$

where $\dot{\varepsilon}_{si}$ is the dielectric function of unexcited crystalline silicon in terms of temperature, and $\dot{\varepsilon}$ is the complex dielectric function, similar to the Drude model of optical response in a homogeneous plasma as follows [17]:

$$\dot{\varepsilon} = \dot{\varepsilon}_{Si} - \left(\frac{\omega_p}{\omega}\right)^2 \frac{1}{1+i\dfrac{1}{\omega\tau_d}} \tag{8}$$

In Eq. (8), ω_p is the plasma frequency, ω is the laser frequency, and τ_d means the electron-electron collision time which is taken as 1.0 fs in this simulation [26].

The finite difference method with the fully implicit scheme is used for solving the governing equations. It is assumed that the electron and lattice temperatures are maintained at 300 K, and the carrier number density is initially set to 1.0×10^{18} m^{-3} [20]. In Fig. 1, which shows a two-dimensional silicon film structure considered in the present study, Neumann conditions are applied at the top and bottom surfaces. Three different film thicknesses of 500 nm, 1.0 μm, and 10 μm are chosen to see the thickness effects, and the wavelength and the beam spot size of the ultrashort pulse laser are taken as 530 nm, and 3.0 μm, respectively, for all cases. The pulse durations are 100 fs and 10 ps with different number of pulses. All physical properties depend on the local temperature and the carrier number density. The physical properties of silicon film are listed in Table 1.

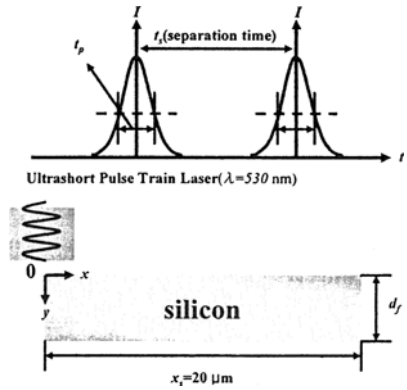

Fig. 1. A schematic of the silicon film structure irradiated by the ultrashort pulse train laser.

Table 1. Physical properties of the silicon film [20].

Property	*Description*
C_e (J/m^{3}K)	$3Nk_B$
C_l (J/m^{3}K)	$1.978\times10^6+(3.54\times10^2)T_l$ $-(3.68\times10^6)T_l^{-2}$
k_e (W/mK)	$-0.556+7.13\times10^{-3}T_e$
k_l (W/mK)	$1.585\times10^5 T_l^{-1.23}$
γ (m^6/s)	3.8×10^{-43}
δ (s^{-1})	$3.6\times10^{-10}\exp(-1.5E_g/k_BT_e)$
D_0 (m^2/s)	$1.8\times10^{-3}(300/T_l)$
E_g (J)	$1.86\times10^{-19}-1.123\times10^{-22}(T_l^2$ $/(T_l+1108))-2.4\times10^{-29}N^{1/3}$
n	$4.159+(5.025\times10^{-4})$ $\times(T_l-300)$
k	$2.13\times10^{-2}\exp(T_l/430)$
τ_{e-l} (ps)	$0.5(1+(N/2.0\times10^{27}))$
α (m^{-1})	$5.02\times10^5\exp(T_l/430)$
θ (m^2)	$5\times10^{-22}(T_l/300)$

3. Results and discussion

Fig. 2 depicts the transient behavior of the carrier number density, the electron and lattice temperatures of a silicon film irradiated by the pico-to-femtosecond pulse train laser at the center (x = 0 and y = 0). The pulse duration times are 10 ps and 100 fs with the laser fluence of 0.2 J/cm^2. As shown in Fig. 1, during the laser irradiation, a nonequilibrium between the electron and lattice temperatures exists because the laser pulse duration is much shorter than the electron-lattice relaxation time, and the electron heat capacity is relatively very small. At the early stage of the laser irradiation, the carrier number density increases substantially because the single-photon absorption energy creates the electrons in the conduction band and the holes in the valence band. As time goes on, the electron and lattice temperatures are in equilibrium through a process of electron-lattice energy relaxation. However, at the short pulse duration (100 fs), the electron and lattice temperatures still remain higher compared to the longer pulse case (10 ps) because the femtosecond pulse lasers have higher peak intensity than the picosecond pulse lasers. Unlike 100 fs, a two-peak structure in the electron temperature distribution at t_p=10 ps appears because both the laser pulse and the rapid Auger recombination heat up the electrons. For the femtosecond laser pulses, the Auger recombination process is not dominant.

The time evolution of the reflectivity at the top surface is illustrated in Fig. 3. It is noted that the reflectivity changes in a pulse duration because of the variation of the electron number density and the temperature. In both cases, the reflectivity decreases at the early stage of the laser irradiation because the real part of the refractive index decreases abruptly. Eventually, it reveals that the reflectivity may be saturated to certain values as can be seen in Fig. 3.

Fig. 4 shows the temporal distributions of the electron and lattice temperatures at the top surface irradiated by a single burst laser at different pulse conditions: (a) a single pulse per train; and (b) three pulses per train, at the total laser fluence of 0.3 J/cm^2.

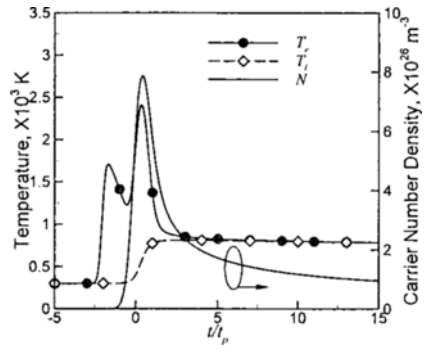

(a) 10 ps

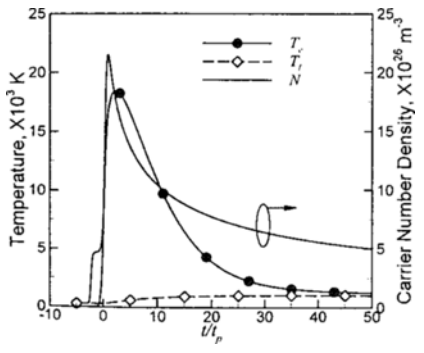

(b) 100 fs

Fig.2. The pulse duration effect on the carrier number density, and the electron and lattice temperatures for 1.0 μm silicon film (thick) at the center.

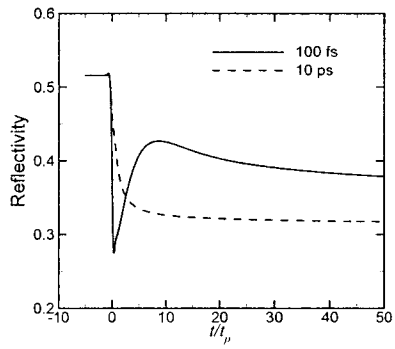

Fig. 3. Estimated reflectivities of silicon film structure during laser irradiation with different laser pulses (single pulse).

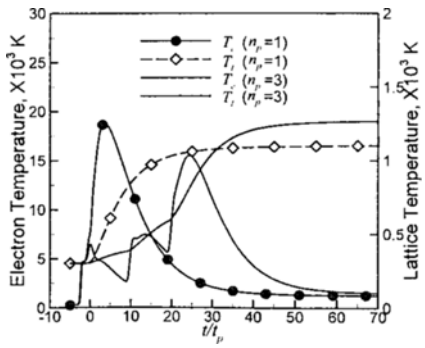

Fig.4. Temporal behaviors of electron and lattice emperatures with a 500 nm thick silicon film at x=0.0 and y=0.0 for different numbers of pulse.

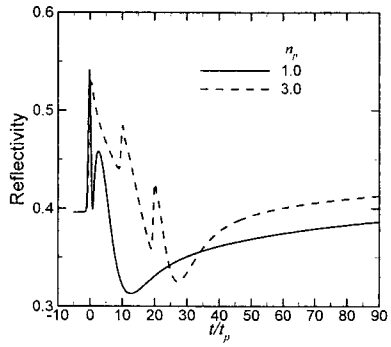

Fig.5. Effect of the number of pulse on reflectivity with a 500 nm thick silicon film at x=0.0 and y=0.0.

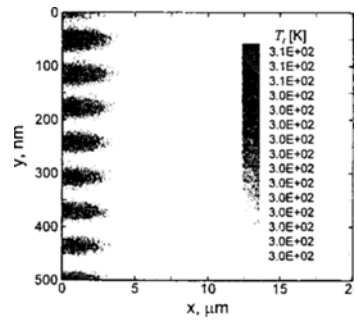

(a) 0.0 ps

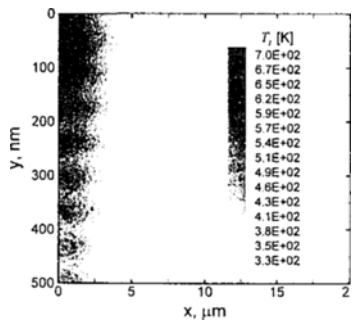

(b) 2.1 ps

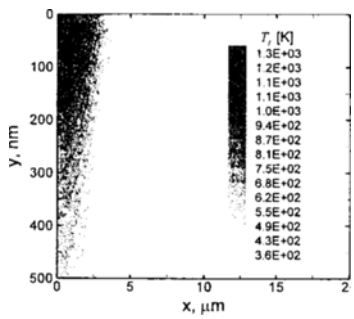

(c) 9.5 ps

Fig. 6. Spatial distributions of lattice temperature after irradiation of three pulses per train.

The separation time is defined as the time interval between two pulses, and its value is chosen as 1.0 ps for both cases as shown in Fig. 1. The peak value of the electron temperature increases gradually because of the incubation effect of the last pulse. Besides, the increasing pattern of the lattice temperature is different for two cases because the laser with three pulses has lower energy absorption at the first and second pulse stages, compared to the single pulse laser. Finally, for the pulse train laser with three pulses, the lattice temperature remains higher than that for the single pulse laser. Furthermore, the variation of the reflectivity for two cases is presented in Fig. 5. In spite of the identical total laser fluence for two cases, the optical characteristics are observed differently during laser heating because before the second stage of the laser irradiation, the optical properties of the silicon film have already been changed by the first laser heating.

Fig. 6 represents the spatial distributions of the lattice temperature for total laser fluence of 0.3 J/cm^2 with three pulses. A two-dimensional silicon film of 20 μm $\times$ 0.5 μm is simulated. To determine the propagation of laser absorption in the silicon film, the present study uses thin film optics, including Eqs. (6) and (7). It is found in Figs. 6(a) and 6(b) that the wave-like propagation of absorption energy can directly affect the spatial distributions of the lattice temperature. Most previous works showed that the carrier number density and the electron and lattice temperatures decrease monotonically along the y direction. However, as the film thickness is comparable to the laser wavelength, the wave-like tendency of energy absorption becomes dominant. For the laser irradiation with three pulses, the lattice temperature shows a wavy profile. As time goes by, as in Fig. 6(c), the profiles of the lattice temperature have a smooth oval form due to the energy relaxation between electrons and lattice phonons.

Fig. 7 depicts the time evolution of the reflectivity and the energy absorption at different thicknesses. In this case, the number of pulses and the pulse duration time are double pulses and 100 fs, respectively. The total laser fluence is taken as 0.4 J/cm^2 for all cases. For film thicknesses of 1.0 μm and 10 μm, the decreasing tendency in the reflectivity can be observed at the instant of the laser irradiation, whereas for 0.5 μm, the reflectivity increases with time as shown in Fig. 7(a). This result is important in determining the amount of laser energy absorbed in

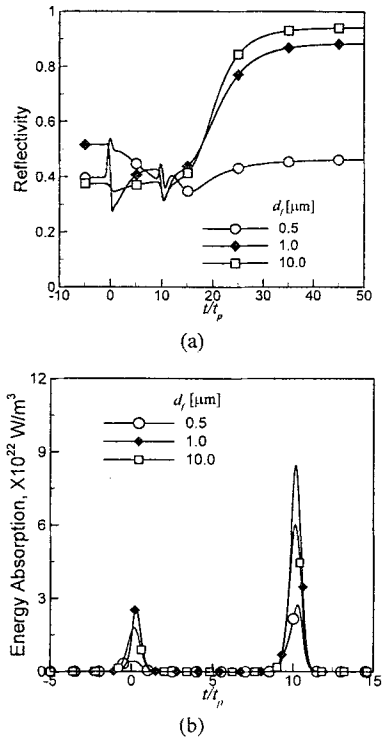

Fig. 7. Effects of film thickness on reflectivity and laser energy absorption at x=0.0 and y=0.0: (a) reflectivity; (b) laser energy absorption.

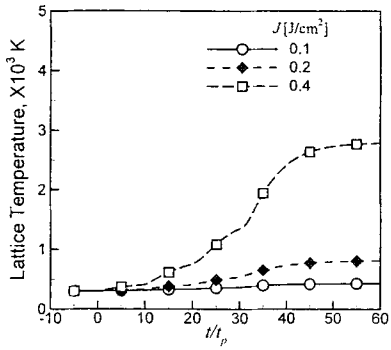

Fig. 8. The temporal behavior of lattice temperature for silicon film irradiated by femtosecond pulse laser with four pulses per train.

the silicon film. In Fig. 7(b), indicating the laser energy absorptions, for a thickness of 0.5 μm, the amount of laser energy becomes the smallest among other cases in the present study. For two cases of 1.0 μm and 10 μm, such metal-like optical characteristics can be seen, indicating that the materials irradiated by the ultrashort pulse train laser undergo a change in optical characteristics like a metal due to the rapid

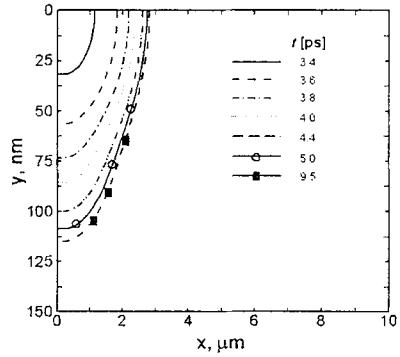

Fig. 9. The estimated crater shapes with respect to time at J = 0.4 J/cm^2.

decrease in the band-gap of silicon.

Fig. 8 shows the variation of the lattice temperature with respect to the laser fluence. The number of pulses is taken as 4 pulses per train. As the laser fluence increases, so does the lattice begin to melt at t = 3.3 ps. Then, the molten zone propagates along both x and y directions as time goes by. As can be seen in Fig. 9, the estimated ablation depth is about 115 nm at t = 9.5 ps.

4. Conclusions

The present study numerically examines the heat transport and the optical characteristics of silicon film structure irradiated by pico to femtosecond pulse train lasers. A two-dimensional and two-temperature model considering wave interference is established to predict the variation of the carrier number density, and the electron and lattice temperatures.

(1) It is confirmed that nonequilibrium between electron and lattice temperatures occurs because the pulse duration time is much shorter than the electron-lattice relaxation time and the electron heat capacity is smaller than that of lattice phonon. In addition, the influence of pulse duration on the carrier density and the electron and lattice temperatures is discussed in detail. For instance, at a 10 ps pulse, a two-peak structure in the temporal distribution of the electron temperature can be observed, whereas for the shorter pulse, a single peak appears.

(2) Unlike a single burst pulse laser irradiation, quite a different tendency can be seen in the carrier number density and temperatures of lattice phonons and electrons when pulse train lasers are irradiated. For example, the maximum electron temperature for three pulses per train becomes lower than that for the

single pulse, whereas in the pulse train laser case, the lattice temperature is higher than the single pulse because the optical and thermal properties are changed with time when the pulse train laser is irradiated on silicon films. This tendency is clearly different from the case of the single pulse laser.

(3) It is found that unlike the bulk silicon, the energy absorption rates are changed significantly with the film thickness. Through the spatial distribution of the lattice temperature, the crater shape and the ablation depth are estimated on the basis of melting temperature of silicon.

Acknowledgements

The authors gratefully acknowledge the financial support from the Micro Thermal System Research Center sponsored by the Korea Science and Engineering Foundation.

Nomenclature

D_0 : Ambipolar diffusivity, m^2/s
d_f : Film thickness, m
E_g : Bandgap energy, J
G : Laser source term, W/m^3
I : Laser intensity, W/m^2
J : Laser fluence, J/cm^2
k : Imaginary part of refractive index
k_B : Boltzmann constant, Js
k_e : Electron thermal conductivity, W/mK
N : Carrier number density, $/m^3$
n : Real part of refractive index
n_p : Number of pulse
R : Reflectivity
$\dot{g}_{tot}$: Total laser source term, W/m^3
r_0 : Laser beam spot size, m
S_m : Poynting vector
T : Temperature, K
t_p : Pulse duration time, s
t_s : Separation time, s
U : Internal energy, J
α : Linear absorption coefficient, /m
β : Two-photon absorption coefficient, m/W
γ : Auger recombination coefficient, m^6/s
δ : Impact ionization coefficient, /s
$\acute{\epsilon}$: Dielectric function
θ : Free carrier absorption coefficient, m^2
λ : Wavelength, m
τ_d : Electron-electron collision time, s
$\tau_{e\text{-}l}$: Electron-lattice relaxation time, s
ω : Laser frequency, /s
ω_p : Plasma frequency, /s
$\hbar$: Reduced Planck constant, Js

Subscripts

e : Electron
l : Lattice

References

[1] D. Bäuerle, Laser processing and chemistry, *Springer*, (2000).

[2] R. Stoian, M. Boyle, A. Thoss, A. Rosenfeld, G. Korn, I. V. Hertel, and E. E. B. Campbell, Laser ablation of dielectrics with temporally shaped femtosecond pulses, *Appl. Phys. Lett.* 80 (2002) 353-355.

[3] M. Lapczyna, K. P. Chen, P. R. Herman, H. W. Tan, and R. S. Marjoribanks, Ultra high repetition rate (133MHz) laser ablation of aluminum with 1:2-ps pulses, *Appl. Phys. A.* 69[Suppl.] (1999) S883-886.

[4] L. Jiang, and H. L. Tsai, Repeatable nanostructures in dielectrics by femtosecond laser pulse trains, *Appl. Phys. Lett.* 87 (2005) 151104~151104-3.

[5] L. Jiang, and H. L. Tsai, Modeling the femtosecond laser pulse-train ablation of dielectrics, *Proceedings of ASME International Mechanical Engineering Congress & Exposition.* (2005).

[6] L. Jiang, and H. L. Tsai, Modeling of ultrashort pulse-train laser heating of metal films, *Proceedings of ASME Heat Transfer Summer Conference,* (2005).

[7] T. Q. Qiu and C. L. Tien, Short-pulse laser heating on metals, *Int. J. Heat Mass Transfer.* 35 (1992) 719-726.

[8] T. Q. Qiu and C. L. Tien, Heat transfer mechanisms during short-pulse laser heating of metals, *ASME J. Heat Transfer.* 115 (1993) 835-841.

[9] T.Q. Qiu, T. Juhasz, C. Suarez, W.E. Bron, and C.L. Tien, Femtosecond laser heating of multi-layer metals-II experiments, *Int. J. Heat Mass Transfer.* 37, 2799–2808 (1994).

[10] D. Y. Tzou, J. K. Chen and J. E. Beraun, Hot-electron blast induced by ultrashort-pulsed lasers in layered media, *Int. J. Heat Mass Transfer.* 40 (1994) 2799-2808.

[11] T. Q. Qiu and C. L. Tien, Femtosecond laser heating of multi-layer metals-I analysis, *Int. J. Heat Mass Transfer.* 37 (1994) 2789-2797.

[12] L. Jiang and H. L. Tsai, Improved two-temperature model and its application in ultrashort laser heating of metal films, *J. Heat Transfer.* 127 (2005) 1167-1173.

[13] E. G. Gamaly, A. V. Rode, B. Luther-Davies and V. T. Thikhonchuk, Ablation of solids by femtosecond lasers; ablation mechanism and ablation thresholds for metals and dielectrics, *Physics of Plasmas.* 9 (2002) 949-957.

[14] K. Eidmann, J. Meyer-ter-Vehn, T. Schlegel, and S. Huller, Hydrodynamic simulation of subpicosecond laser interaction with solid-density matter, *Phys. Rev. E.* 62 (2002)1202-1214.

[15] S. D. Brorson, A. Kazeroonian, J. S. Moodera, D. W. Face, T. K. Cheng, E. P. Ippen, M. S. Dresselhaus and G. Dresselhaus, Femtosecond room-temperature measurement of the electron-phonon coupling constant λ in metallic superconductors, *Phys. Rev. Lett.* 64 (1990) 2173-2175.

[16] J. K. Chen and J. E. Beraun, Modeling of ultrashort laser ablation of gold films in vacuum, *J Opt. A:Pure and Applied Optics.* 5 (2003) 168-173.

[17] Y. Choi and C. P. Grigoropoulos, Plasma and ablation dynamics in ultrafast laser processing of crystalline silicon, *J. Appl. Phys.* 92 (2002) 4918-4925.

[18] S. H. Lee, H. S. Sim, J. Lee, J. M. Kim and Y. E. Shin, Three temperature model for nonequilibrium energy transfer in semiconductor films irradiated by short pulse lasers, *Mat. Trans.* 47 (2006) 2835-2841.

[19] S. H. Lee, J. S. Lee, S. Park and Y. K. Choi, Numerical analysis on heat transfer characteristics of a silicon film irradiated by pico-to femtosecond pulse lasers, *Numerical Heat Transfer Part A.* 44 (2003) 833-850.

[20] H. M. van Driel, Kinetics of high-density plasma generated in Si by 1.06- and 0.53 μm picosecond laser pulse, *Phys. Rev. B.* 35 (1987) 8166-8176.

[21] C. P. Grigoropoulos, H. K. Park and X. Xu, Modeling of pulsed laser irradiation of thin silicon layers, *Int. J. Heat Mass Trans.* 36 (1993) 919-924.

[22] M. Born and W. Wolf, Principles of optics: electromagnetic theory of propagation, interference, and diffraction of light (1980).

[23] H. K. Park, X. Xu, C. P. Grigoropoulos, N. Do, L. Kless, P. T. Leung and A. C. Tam, Temporal profile of optical transmission probe for pulsed-laser heating of amorphous silicon films, *Appl. Phys. Lett.* 61 (1992) 749-751.

[24] I. M. Burakov, N. M. Bulgakova, R. Stoian, A. Rosenfuld and I. V. Hertel, Theoretical investigations of material modification using temporally shaped femtosecond laser pulses, *Appl. Phys. A.* 81 (2005) 1639-1645.

[25] L. D. Landau, E. M. Lifshitz and L. P. Pitaevskii, Electrodynamics of continuous media (1998).

[26] K. Sokoloski-Tinten, D. von der Linde, Generation of dense electron-hole plasmas in silicon, *Phys. Rev. B.* 61 (2000) 2643-2650.